



HAL
open science

InN/InAlN heterostructures for new generation of fast electronics

J. Kuzmik, R. Stoklas, S. Hasenöhrl, E. Dobročka, M. Kučera, P. Eliáš, F. Gucmann, D. Gregušová, Š. Haščík, A. Kaleta, et al.

► **To cite this version:**

J. Kuzmik, R. Stoklas, S. Hasenöhrl, E. Dobročka, M. Kučera, et al.. InN/InAlN heterostructures for new generation of fast electronics. *Journal of Applied Physics*, 2024, 135 (24), 10.1063/5.0215108. hal-04625298

HAL Id: hal-04625298

<https://normandie-univ.hal.science/hal-04625298>

Submitted on 26 Jun 2024

HAL is a multi-disciplinary open access archive for the deposit and dissemination of scientific research documents, whether they are published or not. The documents may come from teaching and research institutions in France or abroad, or from public or private research centers.

L'archive ouverte pluridisciplinaire **HAL**, est destinée au dépôt et à la diffusion de documents scientifiques de niveau recherche, publiés ou non, émanant des établissements d'enseignement et de recherche français ou étrangers, des laboratoires publics ou privés.



Distributed under a Creative Commons Attribution 4.0 International License

InN/InAlN Heterostructures for New Generation of Fast Electronics

J. Kuzmik,^{1*} R. Stoklas,¹ S. Hasenöhr,¹ E. Dobročka,¹ M. Kučera,¹ P. Eliáš,¹ F. Gucmann,¹ D. Gregušová,¹ Š. Haščík,¹ A. Kaleta,² M. P. Chauvat,³ S. Kret,² and P. Ruterana.³

¹Institute of Electrical Engineering, Slovak Academy of Sciences, Dubravská cesta 9, 841 04 Bratislava, Slovakia

²Institute of Physics, PAS, al. Lotnikow 32/46, 02-668 Warsaw, Poland

³Centre de Recherche sur les Ions les Matériaux et la Photonique, UMR CNRS 6252, ENSICAEN, 6 Boulevard Juin, 14050, Caen, France.

Abstract— N-polar InN/In_{0.61}Al_{0.39}N heterostructures are grown directly on a sapphire by using a metal-organic chemical vapor deposition. Thickness of the Mg-doped In_{0.61}Al_{0.39}N is 340 nm, root-mean square surface roughness of the 20-nm thick InN is ~ 3.2 nm. An optional AlN spike grown at 710 °C for 35 s is used either as an interlayer to separate the InAlN buffer from the InN channel or as a part of the InAlN nucleation after sapphire nitridation. High-resolution transmission electron microscopy reveals ~ 2 monolayers of AlN if used as the interlayer. In this case, concentration of screw and edge threading dislocations in partially strained InN decreased down to $6.5 \times 10^9 \text{ cm}^{-2}$ and $38 \times 10^9 \text{ cm}^{-2}$, respectively. More importantly, the interlayer inclusion suppressed remote donor and alloy disorder scatterings, providing at room temperature the InN free electron mobility and concentration of $620 \text{ cm}^2/\text{Vs}$ and $3 \times 10^{13} \text{ cm}^{-2}$, respectively. On the other hand, omitting the AlN spike by InAlN nucleation led to structural deteriorations while buffer resistivity increased to $1.7 \text{ k}\Omega/\square$. Current density of ~ 12-16 A/mm, break-down field of ~ 75 kV/cm and the electron drift velocity of ~ $2 \times 10^7 \text{ cm/s}$ were determined in InN by applying 10-ns voltage pulses on fabricated test resistors.

*Corresponding author. E-mail address: Jan.Kuzmik@savba.sk

Introduction

InN has been recognized as a far-reaching candidate for ultra-high-speed electronics since almost two decades ago [1]. Indeed, very recently these expectations were supported by us extracting the electron drift velocity (v_d) of 1×10^8 cm/s in 775-nm thick molecular-beam epitaxy (MBE)-grown InN, the highest ever reported value in any semiconductor material [2]. High v_d is directly related to transistor cut-off frequency $f_T \sim v_d/2\pi L_G$, where L_G is the gate length [3]. However, mentioned extended layer thickness is not applicable in planar transistor structures and finer designs are needed. Unfortunately, because of the large lattice misfit to typically used GaN templates, thinner InN layers suffer from large density of defects and low electron mobility (μ) [4]. Consequently, no InN-based microwave transistor has been demonstrated yet. Therefore, to mitigate the misfit and InN lattice relaxation, in past we suggested to use In-rich InAlN buffer layer instead of the GaN one [5, 6]. Highly confined electrons of the InN/InAlN quantum well (QW) and strained 5-10-nm thick InN can be expected in this case [5, 6].

Elsewhere we have demonstrated that In-rich InAlN can be grown by a metal-organic chemical vapor deposition (MOCVD) directly on a sapphire, when buffer layer is readily relaxed providing N-polarity and In molar fraction over 0.6 [7, 8]. In our next experiment, 340-nm thick InAlN was followed by a growth of InN channel, reaching μ over 700 cm²/Vs in an InN layer as thin as 20 nm [9]. XRD diffractions indicated clear signals of both of the InAlN buffer and InN channel layers, while by AFM established InN root mean square (RMS) surface roughness was only about 1.3 nm. InN coalescence occurred at 10 nm film thickness, InN background electron concentration (n) was about 2×10^{19} cm⁻³ [9], while an optical band-gap (E_G) determined on alternative, 110-nm thick InN test structure was 0.73 eV [8]. We note however, that because of the high In content and narrow E_G , by us tested InAlN buffers provided degenerate n-type conduction and an un-intentional doping density in a range of 10^{19} cm⁻³ [9, 10]. On the other hand, highly resistive buffer is needed for a transistor proper operation and channel pinch-off. Therefore, in another study, InAlN buffer resistivity was modified by an acceptor doping by introducing Cp₂Mg precursor flow during MOCVD growth [10]. This led to a mobility-controlled resistivity increase via electron scattering on Mg-related complexes of InAlN [10]. Still, InN/InAlN QWs with a resistive

*Corresponding author. E-mail address: Jan.Kuzmik@savba.sk

Mg-doped buffer were not tested till now.

We assume several particular electron scattering mechanisms to influence performance of suggested QWs. In the case of the un-intentionally doped InAlN buffer, apart from the alloy disorder, μ of InN 2-dimensional electron gas (2DEG) will be modulated also by remote donor Coulomb scattering up-to the distance of about 5 nm [11, 12]. Quality of the channel/buffer interface will determine interface roughness scattering [11, 13] while InN channel itself will allocate charged dislocation, ionized impurity and optical phonon scatterings [4, 13-16]. Interestingly, optical phonons could be linked also to premature v_d saturation, particularly in the case of high 2DEG density (N_s) via accumulation of hot phonons [11, 17]. We note that a method of substrate nucleation can also influence 2DEG transport properties by changing the quality of grown layers [18, 19]. Earlier we have shown that sapphire Nitridation at 1010 °C for 300 s combined with AlN nucleation at 730 °C for 30 s led to N-polar growth [7]. On the other hand, dissociation of thin AlON nucleation layer to Al-polar AlN islands might be responsible for an inversion domains formation [18]. Taking this into account and to access all the mentioned scattering phenomena, in this study we prepared InN (20nm)/In_{0.61}Al_{0.39}N (Mg) QWs at slightly reduced temperature of Nitridation & nucleation and with an optional < 1 nm thin AlN interlayer between the buffer and the channel. Additional QW structure without AlN nucleation step has been also prepared. If our proof-ofcept structures validate expectations for InN unique electron transport properties, that might open a way towards new generation of fast electronics.

Recently, N-polar III-N heterostructures attracted considerable attention due to several advantages offered to high-electron mobility transistors (HEMTs), if compared with their metal-polar counterparts [20]. Among them are low-resistance ohmic contacts formed directly on the channel, scalability of the transistor dimensions not limited by the barrier thickness, and reduced short-channel effects provided by their inherent back-barrier [20]. Similar advantages could be expected also by realizing N-polar InN/InAlN HEMTs. Moreover, the polarity provides a possibility to grow InN as the last layer with a relatively low polarization at the surface and without risking a damage during subsequent growth [6]. However, MOCVD of N-polar III-N structures is challenging, particularly because of possible impurity incorporation, such as oxygen, and because of possible inversion domains and threading dislocations

*Corresponding author. E-mail address: Jan.Kuzmik@savba.sk

formation [20, 21]. Vicinal sapphire substrates were successfully applied to handle these issues [20, 21]. In the case of InN however, situation might be more favorable for the N-polar InN because of the higher temperature of the growth if compared with the InN-polar InN [22]. Consequently, while the density of edge-type dislocations of $\sim 1 \mu\text{m}$ thick MBE-grown N-polar InN was about $2 \times 10^{10} \text{ cm}^{-2}$ in the broad temperature range of the growth between $500 \text{ }^\circ\text{C}$ and $600 \text{ }^\circ\text{C}$, that could reach a range of 10^{11} cm^{-2} in the In-polar InN if the substrate temperature was kept at $440 \text{ }^\circ\text{C}$. Similarly, worse structural quality and lower $\mu = 1050\text{-}1850 \text{ cm}^2/\text{Vs}$ were recorded in $\sim 0.8 \mu\text{m}$ thick MBE-grown In-polar InN if compared with $\mu = 1300\text{-}2600 \text{ cm}^2/\text{Vs}$ observed for the N-polar InN [23]. Relatively high temperature of $640 \text{ }^\circ\text{C}$ during the MOCVD growth was probably beneficial also for the N-polar 20-nm thick InN grown on GaN, reaching $\mu = 706 \text{ cm}^2/\text{Vs}$ at RT [24].

Experiment

We used AIXTRON $3 \times 2''$ flip-top close-coupled showerhead reactor for the MOCVD growth, trimethylindium (TMI), trimethylaluminum (TMAI) and ammonia (NH_3) were utilized as In, Al, and N precursors, N_2 was used as a carrier gas. Sapphire substrates were exposed to NH_3 flow for 300 s at $990 \text{ }^\circ\text{C}$, followed by an AlN nucleation spike grown for 35 s at $710 \text{ }^\circ\text{C}$ as a part of sapphire nucleation. 340-nm thick Mg-doped InAlN buffer has been grown at the same temperature using 30 nmol/min Cp_2Mg precursor flow and in-situ baked for 20 min, as described elsewhere [10]. Finally, 20-nm thick InN channel has been grown at $600 \text{ }^\circ\text{C}$ [9]. As an alternative approach to described sample A, the AlN spike was also introduced as an interlayer between the buffer and the channel (sample B), or has been completely omitted (sample C). We note that acceptor-doping of the InAlN buffer can led to redistribution of Mg atoms to the InN channel layer. This can happen either due to reactor memory effect [25], or via various diffusion processes [26, 27]. Elsewhere it was shown that Mg-doped InN electrical and optical properties are only slightly modified if $\text{Cp}_2\text{Mg}/(\text{TMI})$ flow ratio during the InN growth $< 4 \times 10^{-2}$ [28]. This may implicate that properties of our nominally undoped InN is not much affected by diffusion from the grown InAlN (when flow ratio $\text{Cp}_2\text{Mg}/(\text{TMAI} + \text{TMI}) = 1.9 \times 10^{-3}$), apart from the fact that Mg-

*Corresponding author. E-mail address: Jan.Kuzmik@savba.sk

memory effect might be suppressed by 20 min baking before the InN growth.

High-resolution X-ray diffraction (HR-XRD) measurements were performed using Bruker D8 DISCOVER diffractometer equipped with rotating Cu anode and operating at 12 kW. Diffractions 0004 and $11\bar{2}4$ were measured to determine In molar fraction, lattice parameters, and strain states. We estimate the uncertainty of the measured 2θ angles of the InAlN and InN diffractions, and of the signal FWHM to be 0.0005° , 0.006° and 0.02° , respectively. The density of dislocations (N_{dis}) with screw (N_{disS}) and edge components (N_{disE}) was evaluated from the X-ray rocking curves [9]. NT-MDT NTEGRA Prima atomic force microscope (AFM) in tapping mode and FEI Quanta 250 FEG scanning electron microscope (SEM) were used to study surface morphology of grown samples. High-resolution transmission electron microscopy (HRTEM) was carried out in an FEI CUBED TITAN microscope equipped with a monochromator and a spherical aberration (Cs) corrected objective lens. The negative Cs mode, which permits to image also light elements, has been used to determine the polarity of the layers. The analysis of the layers crystallographic quality was carried out in the weak beam mode using a JEOL F200 microscope. Photoluminescence (PL) spectra of the InAlN buffer layers were measured at 6.5 K using a 488 nm line of an Ar + laser as a pump and a silicon photodiode for the detection of PL radiation. Hall transport parameters were measured in the temperature (T) range between room temperature (RT) and 4 K in the standard Van der Pauw configuration. Energy band diagram and free electron concentration profile of studied heterostructures were calculated using a Schrödinger-Poisson equation solver [29].

To assess QWs electrical performance, we prepared specific test structures consisting tiny planar resistors ($6\ \mu\text{m}$ length / $2 \times 16\ \mu\text{m}$ width, fed with ohmic contacts in a coplanar arrangement) formed by a plasma etching and Ohmic contacts formation. For extracting current-voltage characteristics, we applied 10-ns long voltage pulses with a duty cycle 0.01 generated by HP 8114A. Consequently, v_d could be calculated as I/qN_s , where I is the current density and q is the electron charge [2]. Pulsed probing was necessary to eliminate the self-heating and premature burnout of structures [30].

*Corresponding author. E-mail address: Jan.Kuzmik@savba.sk

Results and discussion

Figure 1 shows XRD 0002 $2\theta/\omega$ diffractions of investigated samples. Table 1 summarizes material parameters determined also by supplementary XRD scans, with x_{InN} representing content of InN, ε_l in-plane strain, with full-width-half maxima (FWHM) of corresponding diffractions and with calculated dislocation densities. x_{InN} of the InAlN buffer layer was found to be between 60 % and 61 %, x_{InN} of the InN channel between 98 % and 99 % may reflect ambiguity of the extraction method and/or possible contamination of the layer.

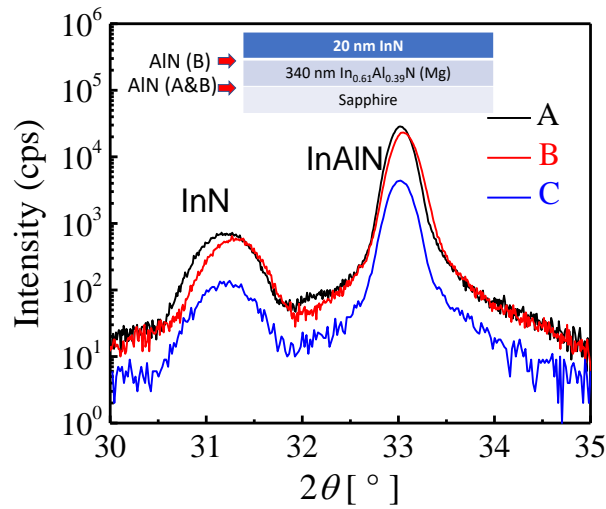


Fig. 1. XRD $2\theta/\omega$ diffraction curves of InN(20 nm)/In_{0.61}Al_{0.39}N (Mg) samples A-C grown on c-plane sapphire. Inset shows sketch of the heterostructure with optional AlN spikes.

Table 1. Material parameters of samples A-C extracted from XRD experiments. The numbers in the parentheses mark uncertainties of extractions.

Sample	Layer	X_{InN} (%)	ε_I (%)	FWHM ($^\circ$)			N_{dis} (10^9 cm^{-2})	
				0002	10 $\bar{1}$ 1	10 $\bar{1}$ 0	N_{disS}	N_{disE}
A	InAlN	61(\pm 1)	-0.03	0.28	0.79	0.88	2.0(\pm 0.1)	50(\pm 1)
	InN	99(\pm 1)	-0.8	0.59	0.91	0.98	7.5(\pm 0.2)	54(\pm 1)
B	InAlN	61(\pm 1)	0.04	0.28	0.80	0.90	2.0(\pm 0.1)	50(\pm 1)
	InN	99(\pm 1)	-0.5	0.55	0.77	0.82	6.5(\pm 0.2)	38(\pm 1)
C	InAlN	60(\pm 1)	-0.2	0.35	0.82	0.91	3.0(\pm 0.2)	51(\pm 1)
	InN	98(\pm 1)	-0.7	0.65	0.97	1.05	9.0(\pm 0.3)	62(\pm 1)

Based on the data of Tab. 1 we conclude that by inserting the AlN interlayer between the buffer and the channel of sample B, InN crystallographic quality has improved if compared with sample A. This was reflected by smaller InN diffraction peak FWHM and by lower N_{dis} , down to about $6.5 \times 10^9 \text{ cm}^{-2}$ and $38 \times 10^9 \text{ cm}^{-2}$ of N_{disS} and N_{disE} components, respectively. Simultaneously, ε_I of InN was reduced down to -0.5 %, representing relaxation over 90 % [9]. This is documented also in Figure 1 by sample B InN diffraction maxima shift closer to InAlN, if compared with sample A. On the other hand, in sample C both InN and InAlN layers crystallographic quality deteriorated if AlN nucleation spike was omitted. This is reflected by reduced diffraction signal shown in Figure 1 and by up-to 65 % increase of N_{dis} listed in Tab.1, if compared with samples A and B. Nevertheless, Tab.1 indicates that AlN spike used neither as the interlayer between the buffer and the channel, nor as a part of the nucleation has any influence on X_{InN} , which is about 61 % in the buffer layer and about 99 % in the channel.

Higher level of crystallographic disorder of sample C is also evidenced by PL experiment shown in Figure 2, with broader FWHM of about 279 meV and reduced intensity of PL radiation, likely due to additional non-radiative defects, if compared with sample A. We note invariant position of the PL signal maxima at 1.58 eV, in agreement with determined $X_{InN} \sim 61$ % and expected bandgap bowing [31].

*Corresponding author. E-mail address: Jan.Kuzmik@savba.sk

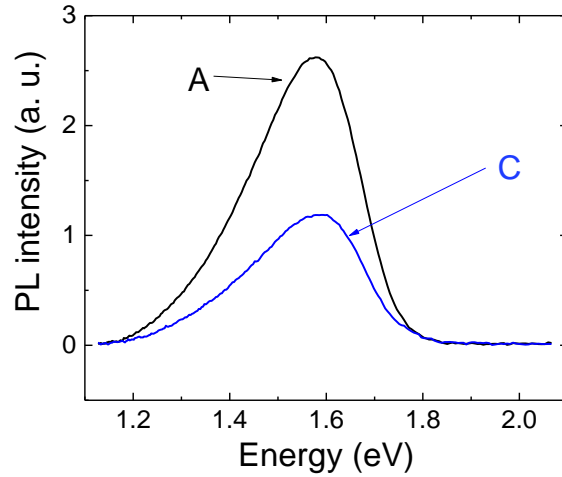


Fig. 2. PL signals of the buffer of samples A and C with and without AlN nucleation spike taken at 6.5 K.

For better understanding of InN/InAlN QWs growth and performance and the role of particular AlN spikes, we further performed SEM, AFM, HRTEM, Hall and I - V experiments. InN surface inspections by SEM are shown in Figure 3. In sample A we noticed relatively compact surface but with occasional cracks. On the other hand, surface of sample B which is less continuous with occasional voids, contains no cracks. We link this phenomenon to AlN interlayer of sample B, providing faster InN relaxation, as indicated also by reduced ε_I in Tab.1. On the other hand, Sample B could probably suffer from InN less mobile adatoms or less dense nucleation sites. Surprisingly, the highest surface quality can be suggested for sample C without any AlN spikes, even though with the highest N_{dis} off the less optimized growth. We speculate that dislocations in the buffer of sample C could provide additional relaxation sites for InN, even though as revealed below, high N_{dis} deteriorates electrical performance. Our conclusions were further supported by AFM $2 \times 2 \mu\text{m}^2$ scans shown in Figure 4. We noticed similar root-mean square (RMS) roughness of about 3.2 nm for all samples however, InN terraces which indicate 2-D growth mode of highly mobile adatoms became less obvious for sample B. Moreover, tiny islands were observed on the surface of sample B, which is probably also linked to the presence AlN interlayer and modified InN growth mode.

*Corresponding author. E-mail address: Jan.Kuzmik@savba.sk

This is the author's peer reviewed, accepted manuscript. However, the online version of record will be different from this version once it has been copyedited and typeset.
PLEASE CITE THIS ARTICLE AS DOI: 10.1063/5.0215108

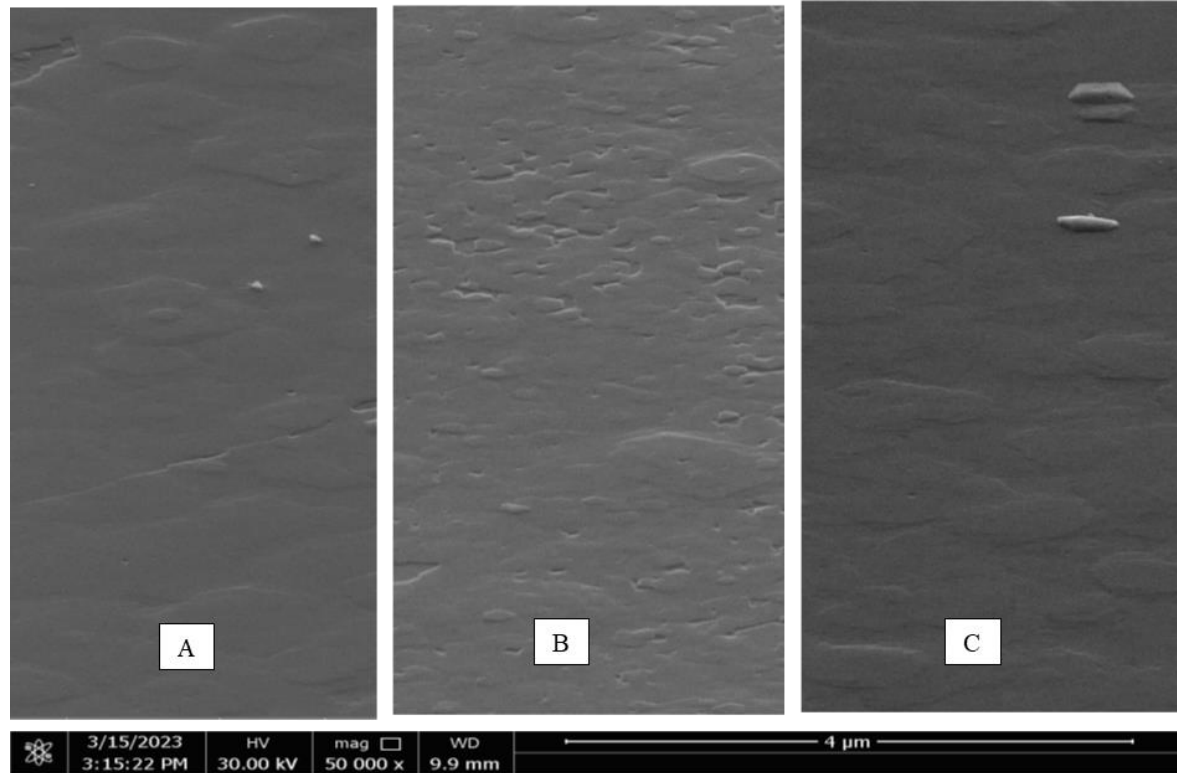


Fig. 3. SEM images of InN(20 nm)/In_{0.61}Al_{0.39}N (Mg) samples A-C.

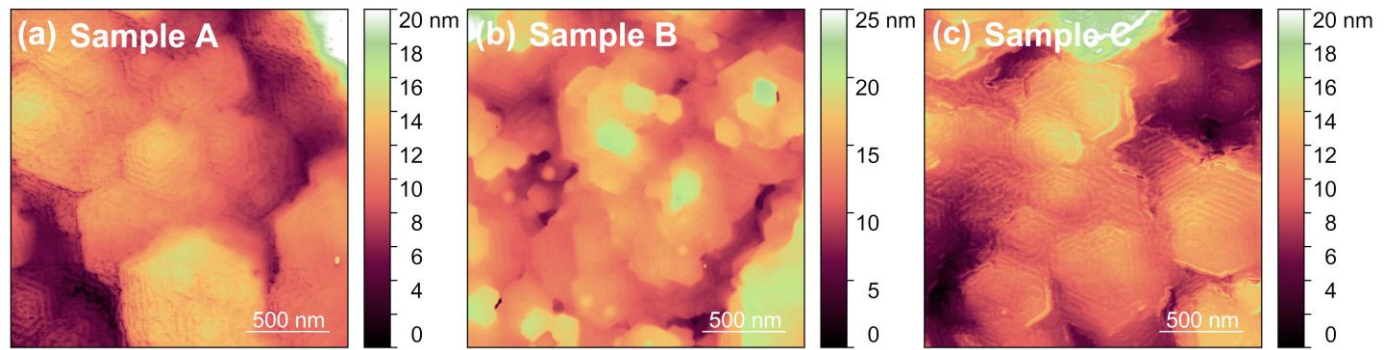


Fig. 4. $2 \times 2 \mu\text{m}^2$ AFM scans of InN(20 nm)/In_{0.61}Al_{0.39}N (Mg). (a) sample A, (b) sample B, (c) sample C.

HRTEM experiments shown in Figure 5 provided vertical inspections. Sample A in Figure 5(a) suggests well-defined InN/In_{0.61}Al_{0.39}N QW interface, with only occasional misfit dislocations. Similar

*Corresponding author. E-mail address: Jan.Kuzmik@savba.sk

investigation of sample B, shown in Figure 5(b), proved additional presence of ~ 2 monolayers of AlN interlayer however, misfit dislocations became less detectable. Nevertheless, all samples demonstrated N-polarity without inversion domains, as exemplified also by the most magnified InN image shown in Figure 5(c).

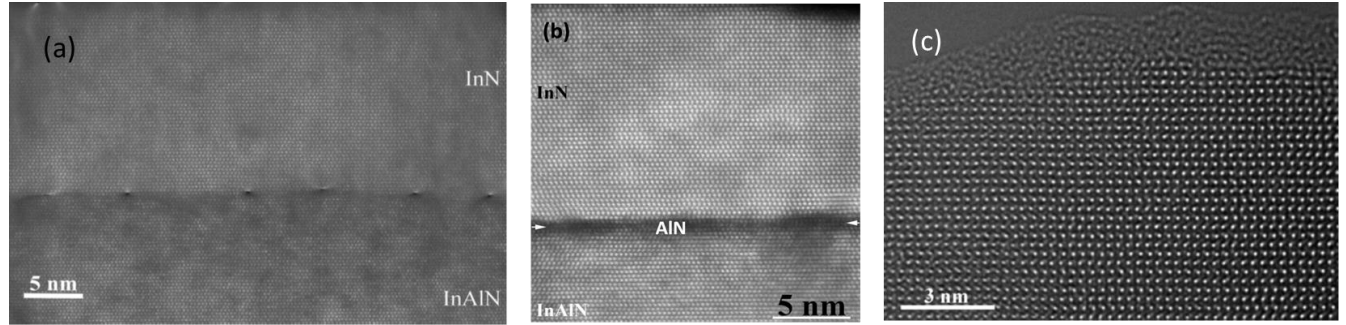


Fig. 5. InN(20 nm)/(AlN)/In_{0.61}Al_{0.39}N (Mg) quantum well heterostructure HRTEM analysis of (a) sample A without and (b) sample B with the inserted AlN interlayer. (c) Detailed view of the N-polarity InN.

To study a role of all above mentioned structural peculiarities in the InN/InAlN QW electron transport properties, next we proceeded with the Hall effect analysis. We note that even though present experiment uses resistive Mg-doped InAlN buffers, some parasitic conduction cannot be completely excluded. Therefore, to determine conduction through the InN channel alone, initial characterization of sole buffer layers followed by a parallel conduction analysis of the whole QW might be needed, similarly as performed elsewhere for QW with un-doped InAlN buffers [9]. As for the buffer layer of samples A and B, here we use our earlier data, i.e. $\mu \sim 5.6 \text{ cm}^2/\text{Vs}$ and $n \sim 6.3 \times 10^{19} \text{ cm}^{-3}$ at RT, down to $\mu \sim 4.7 \text{ cm}^2/\text{Vs}$ and $n \sim 6.5 \times 10^{19} \text{ cm}^{-3}$ at 4 K [10]. Analysis of the buffer layer grown without AlN nucleation (sample C) reveals additional $\sim 15\%$ decrease in μ , and $\sim 50\%$ decrease of n (not shown). That provided increase of the buffer sheet resistance from about $0.7 \text{ k}\Omega/\square$ of samples A and B to $1.7 \text{ k}\Omega/\square$ of sample C. Taking this into account and after finalizing the above-mentioned parallel conduction analysis, we could extract InN/InAlN QW μ and N_s quantities of all samples, shown in Figure 6. We may ascertain that μ of all

*Corresponding author. E-mail address: Jan.Kuzmik@savba.sk

samples increases with decreased T , with a tendency to saturate at $T < 100$ K. This suggests ionized impurity, charge dislocation and interface roughness scattering at low T , with gradual contribution from the polar optical phonon scattering at higher T , similarly as observed for InN elsewhere [13, 15]. From the other point of view, when comparing samples A and B, we noticed a substantial (by ~ 30 %) improvement of μ if InN channel was separated from the buffer by using the AlN interlayer. Therefore, specifically for our case of ternary InAlN buffer layer with high un-intentional doping, we may list InAlN alloy disorder and remote donor scattering among other important aspects of proposed QWs. Interestingly, for sample C, μ remains high even though crystallographic quality suffered from missing AlN nucleation spike, documented by the highest N_{dis} , see Tab.1 and degraded PL, shown in Figure 2. On the other hand, elsewhere it was suggested that dislocations may act also as acceptor states [16]. If we assume the same, dislocations in sample C may compensate the un-intentional doping of InAlN, as suggested by the above observed 50 % drop of n . Consequently, reduced remote donor scattering can also explain high μ of sample C.

We noticed almost T -independent N_s values, shown in Figure 6(b), which were ~ 4 to $5 \times 10^{13} \text{ cm}^{-2}$ for samples A and C without the AlN interlayer. N_s surprisingly dropped to $\sim 3 \times 10^{13} \text{ cm}^{-2}$ for sample B, even though better 2DEG confinement should be provided with the interlayer insertion [5]. Next, for better understanding of all phenomena, we calculated energy band diagrams and electron concentration profiles of suggested QWs, shown in Figure 7. We note that calculations of sample C are not shown here as being almost identical to sample A. At the surface of all samples, our model reflects expected Fermi level (E_F) pinning ~ 1.6 eV above the valence band (E_V) and consecutive electron accumulation [32]. Strongly confined but from the buffer separated 2DEG is shown in Figure 7(b) for sample B. That is in agreement and explain our earlier comments on reduced remote donor and alloy disorder scatterings in this case. Another interesting aspect of sample B is, that the AlN interlayer provides strong lifting of the buffer E_C above E_F close to the interface, see Figure 7(b). That may on one side provide a beneficial ~ 5 -nm thick energy barrier for the electron injection from the InN channel to InAlN, but also an ambiguity in justifying applied parallel conduction analysis. Consequently, N_s values of sample B shown in Figure 6(b) might be underestimated.

*Corresponding author. E-mail address: Jan.Kuzmik@savba.sk

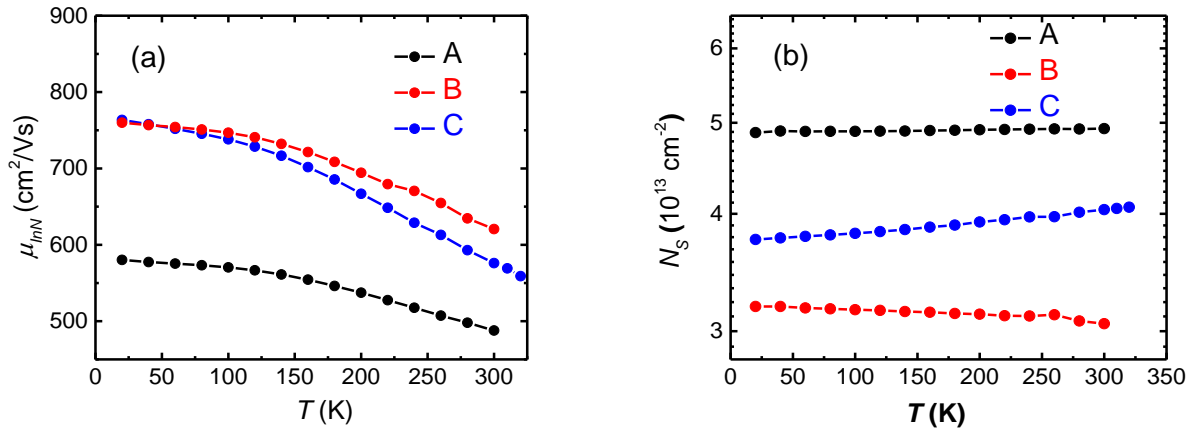


Fig. 6. Hall effect analyses of samples A-C with (a) free electron mobility and (b) carrier concentration values down to 4 K.

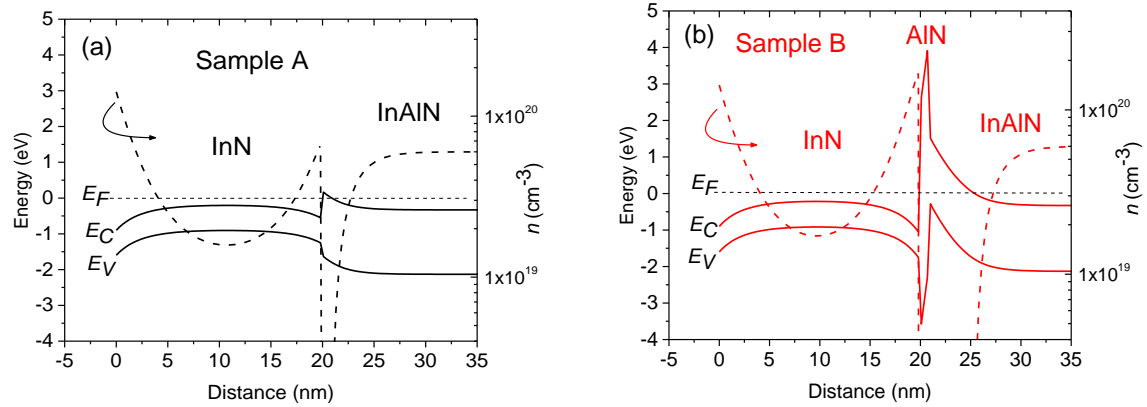


Fig. 7. Calculated energy band diagram and free electron concentration profile of (a) sample A and (b) sample B. All layers were considered to be relaxed, materials parameters were taken from [6, 31].

In Figure 8 we show I - V characteristics of InN/InAlN QW test resistors obtained by using 10-ns long pulses. High current densities, up-to 17 A/mm were obtained, with a tendency to saturate at an electric field (E_{sat}) of ~ 35 kV/cm and with a break-down field (E_{break}) at ~ 70 kV/cm. We note that observed E_{sat} corresponds well with earlier Monte Carlo simulations on electron transport in InN [33, 34], while to our knowledge, there are practically no data on E_{break} in InN. We consider the observed E_{break} to be very

*Corresponding author. E-mail address: Jan.Kuzmik@savba.sk

promising, compared to significantly lower E_{break} of 20 kV/cm of analogous “high-speed” semiconductor material of InAs [35]. Moreover, taking into account dissipated power of ~ 20 W, duration of the pulse, resistor area and our previous selfheating extractions in GaN structures [30], we can estimate temperature to reach > 400 °C at the end of the pulse. This already approaches thermal stability limit of InN [36] indicating that even higher E_{break} could be expected with better cooling. We note also that despite high N_s , the lowest $I \sim 10$ A/mm has been observed for sample A. Reason for that is unknown, we speculate that enhanced accumulation of hot phonons due to high N_s combined with high n in the buffer of sample A might be responsible.

In Figure 9 we show calculated v_d of all samples; buffer conduction was subtracted from I values before each v_d extraction. Samples B and C behave rather similarly, reaching the best $v_d \sim 2 \times 10^7$ cm/s. We account these comparable improvements to AlN spacer insertion in sample B and to reduced n in the buffer of sample C. None of these improvements were applied in sample A and thus, only limited v_d of $\sim 1 \times 10^7$ cm/s was extracted in this case. Nevertheless, obtained $v_d \sim 2 \times 10^7$ cm/s is very promising, taking into account much lower $v_d \sim 1 \times 10^6 - 1 \times 10^7$ cm/s of AlGaIn/GaN QWs [37]. Still, we were not reaching $v_d \sim 1 \times 10^8$ cm/s as reported earlier by us for 770-nm thick InN [2]. This might account to several phenomena of thin films, such as pronounced surface effects, higher background doping, higher N_{dis} , and much lower μ compared to earlier reported value of thick InN, i.e. 1940 cm²/Vs at RT. We may also point on some ambiguity in the v_d extraction related to different conditions of the Hall effect measurement, performed at ~ 200 meV bias and in the steady-state, versus up-to 70 kV/cm transients of pulsed I - V s. Earlier we have suggested that carrier injection in AlGaIn/GaN QWs might lead to gradual surface charging and v_d reduction [37], which was not analyzed in our study. Similarly, surface/interface electron accumulation in InN (shown in Figure 7) might also lead to apparent v_d reduction if additional parallel conduction analysis is neglected [2].

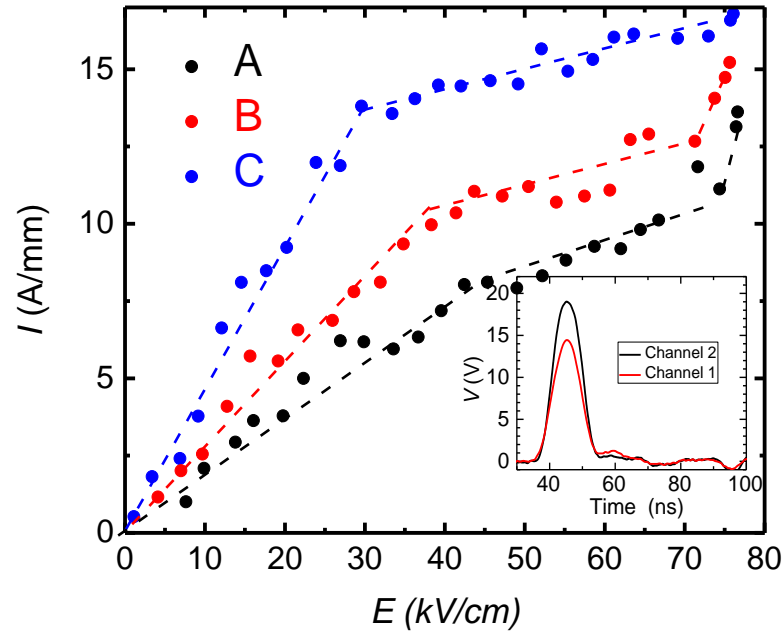


Fig. 8. Pulsed I - V dependences of all samples A-C. Dashed lines interpolate measured points. Inset shows typical 10-ns long waveforms taken by a two-channel oscilloscope.

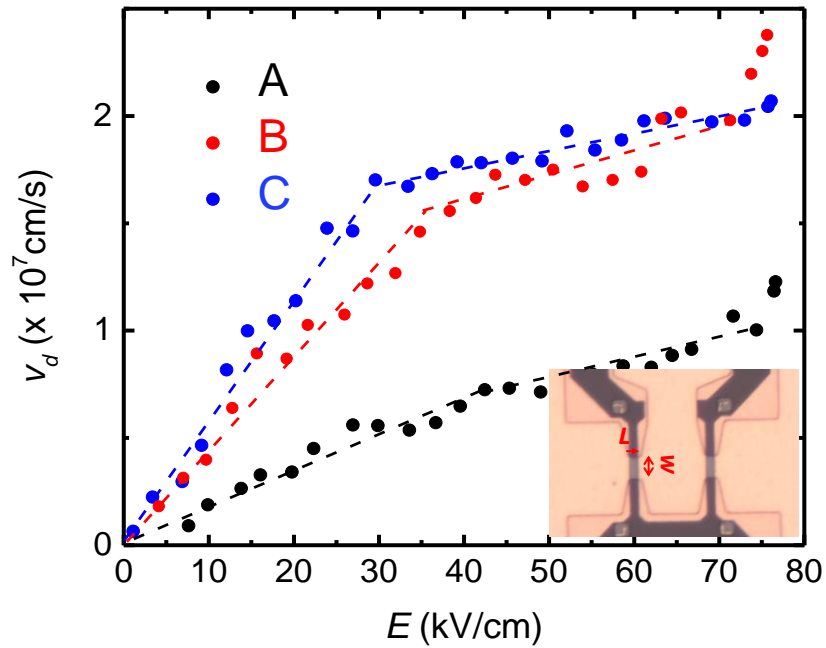


Fig. 9. Extracted electron drift velocity along the 20-nm thick InN channel of samples A-C. Dashed lines interpolate measured points. Inset shows optical microscope view of a 6- μ m long (L) and 2 \times 16- μ m wide

(w) test resistor. Non-alloyed Ti/Al/Ni/Au ohmic contacts and bottom sapphire surface exposed by dry etching are clearly distinguishable.

Conclusion

In conclusion, we report proof-of-concept N-polar InN/In_{0.61}Al_{0.39}N QW heterostructures. 20-nm thick InN has been MOCVD grown on Mg-doped InAlN buffer with an optional AlN spike as an interlayer between the InAlN buffer and the InN channel, or as a part of InAlN nucleation on sapphire. AlN inclusion as an interlayer between the buffer and the channel brought clear improvements, reaching $N_S \sim 4 \times 10^{13} \text{ cm}^{-2}$ and $\mu \sim 620 \text{ cm}^2/\text{Vs}$ at RT, and N_{disS} and N_{disE} of InN as low as $\sim 6.5 \times 10^9 \text{ cm}^{-2}$ and $38 \times 10^9 \text{ cm}^{-2}$, respectively. Remote donors and alloy disorder have been determined as major scattering sources originating in the InAlN buffer, while dislocations and optical phonon scattering were suggested to be decisive in the InN channel itself. If nucleation AlN spike was skipped, InAlN structural quality deteriorated however, buffer resistivity increases. Pulsed I - V characterizations indicated current saturation at $\sim 35 \text{ kV/cm}$, breakdown field of $\sim 70 \text{ kV/cm}$ and v_d of InN electrons to reach at least $2 \times 10^7 \text{ cm/s}$. Our findings prove potential of InN/InAlN QW heterostructures for a future generation of fast electronics. Further developments call for improved InAlN epitaxy with less free electrons and/or better donor compensation, for InN with less N_{dis} and for surface accumulation suppression.

Acknowledgments

This work was supported by VEGA grants no. 2/005/22 and 2/0068/21, and by APVV Agency grant no. APVV-21-0008.

Data availability

The data that support the findings of this study are available from the corresponding author upon reasonable request.

*Corresponding author. E-mail address: Jan.Kuzmik@savba.sk

- [1] S. K. O'Leary, B. E. Foutz, M. S. Shur, L. F. Eastman, *Appl. Phys. Lett.* **88**, 152113 (2006).
- [2] J. Kuzmik, A. Adikimenakis, M. Ľapajna, D. Gregušová, Š. Haščík, E. Dobročka, K. Tsagaraki, R. Stoklas, and A. Georgakilas, *AIP Advances* **11**, 125325 (2021).
- [3] S. M. Sze, K. K. Ng, *Physics of Semiconductor Devices*, 3rd ed. (Wiley, 2007) pp. 347-348.
- [4] A. Adikimenakis, P. Chatzopoulou, G. P. Dimitrakopoulos, Th. Kehagias, K. Tsagaraki, M. Androulidaki, G. Doundoulakis, J. Kuzmik and A. Georgakilas, *ECS J. of Solid-State Sci. and Technol.* **9**, 015006 (2020).
- [5] J. Kuzmik and A. Georgakilas, *IEEE Trans. On El. Dev.* **58**, 720 (2011).
- [6] J. Kuzmik, *Appl. Phys. Express* **5**, 044101 (2012).
- [7] P. Chauhan, S. Hasenöhrl, E. Dobročka, M. P. Chauvat, A. Minj, F. Gucmann, E. Vančo, J. Kováč, Jr., S. Kret, P. Ruterana, M. Kuball, P. Šiffalovič, and J. Kuzmik, *J. Appl. Phys.* **125**, 105304 (2019).
- [8] F. Gucmann, M. Kučera, S. Hasenöhrl, P. Eliáš, A. Rosová, E. Dobročka, R. Stoklas, and J. Kuzmík, *Semicond. Sci. Technol.* **36**, 075025 (2021).
- [9] S. Hasenöhrl, E. Dobročka, R. Stoklas, F. Gucmann, A. Rosová, and J. Kuzmík, *Phys. Status Solidi (a)* **217**, 2000197 (2020).
- [10] J. Kuzmík, O. Pohorelec, S. Hasenöhrl, M. Blaho, R. Stoklas, E. Dobročka, A. Rosová, M. Kučera, F. Gucmann, D. Gregušová, M. Precner, and A. Vincze, *Materials* **16**, 2250 (2023).
- [11] D. Jena, *Quantum Physics of Semiconductor Materials and Devices* (Oxford University Press, 2022) pp. 555-608.
- [12] Ch. Hamaguchi, *J. Appl. Phys.* **130**, 125701 (2021).
- [13] I. Sanyal, Y.-Ch. Chen, Ch.-Y. Yu, and J.-I. Chyi, *J. Appl. Phys.* **134**, 085702 (2023).
- [14] L. Hsu, R.E. Jones, S. X. Li, K. M. Yu, W. Walukiewicz, *J. Appl. Phys.* **102**, 073705 (2007).
- [15] K. Wang, Y. Cao, J. Simon, J. Zhang, A. Mintairov, J. Merz, D. Hall, T. Kosel, and D. Jena, *Appl. Phys. Lett.* **89**, 162110 (2006).
- [16] E. C. H. Kyle, S. W. Kaun, P. G. Burke, F. Wu, Y.-R. Wu, and J. S. Speck, *J. Appl. Phys.* **115**, 193702 (2014).
- [17] L. Ardaravičius, O. Kiprijanovič, J. Liberis, E. Šermukšnis, A. Matulionis, R. A. Ferreyra, A.

- Avrutin, U. Ozgur and H. Morkoc, *Semicond. Sci. Technol.* **30**, 105016 (2015).
- [18] P. Chauhan, S. Hasenöhrl, A. Minj, M. P. Chauvat, P. Ruterana, J. Kuzmik, *Appl. Surf. Sci.* **502**, 144086 (2020).
- [19] M. E. Twigg, D. D. Koleske, A. E. Wickenden, R. L. Henry, and S. C. Binari, *Appl. Phys. Lett.* **79**, 4322 (2001).
- [20] M. H. Wong, S. Keller, Nidhi, S. Dasgupta, D. J. Denninghoff, S. Kolluri, D. F. Brown, J. Lu, N. A. Fichtenbaum, E. Ahmedi, U. Singiseti, A. Chini, S. Rajan, S. P. DenBaars, J. S. Speck, and U. K. Mishra, *Semicond. Sci. Technol.* **28**, 074009 (2013).
- [21] S. Keller, H. Li, M. Laurent, Y. Hu, N. Pfaff, J. Lu, D. F. Brown, N. A. Fichtenbaum, J. S. Speck, S. P. DenBaars, and U. K. Mishra, *Semicond. Sci. Technol.* **29**, 113001 (2014).
- [22] C. S. Gallinat, G. Koblmüller, F. Wu, and J. S. Speck, *J. Appl. Phys.* **107**, 053517 (2010).
- [23] T. A. Komissarova, E. Kampert, J. Law, V. N. Jmerik, P. Paturi, X. Wang, A. Yoshikawa, and S. V. Ivanov, *Appl. Phys. Lett.* **112**, 022104 (2018).
- [24] C. Lund, M. Catalano, L. Wang, Ch. Wurm, T. Mates, M. Kim, S. Nakamura, S. P. DenBaars, U. K. Mishra, and S. Keller, *J. Appl. Phys.* **123**, 055702 (2018).
- [25] Y. Ohba, A. Hatano, *J. Crystal Growth* **145**, 214 (1994).
- [26] A. Agarwal, M. Tahhan, T. Mates, S. Keller, and U. Mishra, *J. Appl. Phys.* **121**, 025106 (2017).
- [27] W. Yi, A. Kumar, J. Uzuhashi, T. Kimura, R. Tanaka, S. Takashima, M. Edo, Y. Yao, Y. Ishikawa, J. Chen, T. Ohkubo, T. Sekiguchi, and K. Hono, *Appl. Phys. Lett.* **116**, 242103 (2020).
- [28] A. Yamamoto, Y. Nagai, H. Niwa, H. Miwa, A. Hashimoto, *J. Crystal Growth* **298**, 399 (2007).
- [29] I. H. Tan, G. L. Snider, E. L. Hu, *J. Appl. Phys.* **68**, 4071 (1990).
- [30] J. Kuzmik, S. Bychikhin, M. Neuburger, A. Dadgar, A. Krost, E. Kohn, and D. Pogany, *IEEE Trans. On El. Dev.* **52**, 1698 (2005).
- [31] Hasenöhrl, S., Blaho, M., Dobročka, E., Guemann, F., Kučera, M., Nádaždy, P., Stoklas, R., Rosová, A., and Kuzmík, J.: *Mater. Sci Semicond. Process.* **156**, 107290 (2023).
- [32] J. Kuzmík, Š. Haščík, M. Kučera, R. Kúdela, E. Dobročka, A. Adikimenakis, M. Mičušík, M. Gregor, Plecenik, A. Georgakilas, *Applied Phys. Lett.* **107** 191605 (2015).

This is the author's peer reviewed, accepted manuscript. However, the online version of record will be different from this version once it has been copyedited and typeset.
PLEASE CITE THIS ARTICLE AS DOI: 10.1063/5.0215108

- [33] V. M. Polyakov and F. Schwierz, Appl. Phys. Lett. **88**, 032101 (2006).
- [34] W. A. Hadi, P. K. Guram, M. S. Shur, and S. K. O'Leary, J. Appl. Phys. **113**, 113709 (2013).
- [35] X. Li, K. F. Longenbach, Y. Wang, W. I. Wang, IEEE El. Dev. Lett. **13**, 192 (1992).
- [36] M. Kučera, A. Adikimenakis, E. Dobročka, R. Kúdela, M. Ťapajna, A. Laurenčíková, A. Georgakilas, and J. Kuzmík, Thin Solid Films **672**, 114 (2019).
- [37] J. Kuzmík, S. Bychikhin, D. Pogany, C. Gaquiere, E. Morvan, J. Applied Phys. **99** 123720 (2006).